Underwater Full-Duplex 4 × 4 MIMO Optical Communication System Based on Imaging Reception

Yanlong Li, Shuaixing Li, Xiao Chen, Tuyang Wang(✉), and Yutong Jiang

Ministry of Education Key Laboratory of Cognitive Radio and Information Processing, School of Information and Communication, Guilin University of Electronic Technology, Guilin 541004, China

tuyangwang@guet.edu.cn

Abstract. In recent years, with the continuous exploitation of marine resources around the world, the problem of underwater data communication has gradually become a research hotspot. This paper establishes an optical domain transmitting imaging reception model and proposes a MIMO communication system based on it, which the received spot must be aligned with the detector arrays. Moreover, it designs a transmission system based on this model by FPGA to complete real-time signal processing. However, the physical movement, turbulence, and other causes of the transceiver link misalignment will make the light spot offset the detector target surface, thus reducing the receive signal-to-noise ratio (SNR) and limiting the transmission distance. So, this system uses optical fiber to couple the received optical signal to the detector arrays, which reduces the alignment requirements. Further, we propose a Lattice Reduction zero forcing (LLL-ZF) detection algorithm for MIMO signal detection, which can reduce interference effectively. This imaging reception mode and MIMO signal detection can reduce the mutual interference between sub-links and decrease the complexity of the detection algorithm. The experimental results show that when the system's BER is less than the FEC threshold value at a communication distance of 30 m underwater, the sub-channel communication rate of the system can reach 20 Mbps and the 4 × 4 MIMO system rate can reach 80 Mbps.

Keywords: Underwater optical communication · Imaging MIMO · Plano-convex lens · Fiber optic coupling · Lattice Reduction

1 Introduction

In recent years, underwater wireless communication (UWC) technology has been in increasing demand with the exploration and exploitation of marine resources [1]. Currently, underwater wireless communication methods are divided into three main categories: underwater acoustic communication (UAC) [2], underwater radio frequency (RF), and underwater optical communication (UWOC) [3]. Hydroacoustic communication has been developed as a more mature communication method for many years.

J. Wang (Ed.): MobiMedia 2023, LNICST 576, pp. 96–109, 2025.
https://doi.org/10.1007/978-3-031-60347-1_10

However, due to the narrow bandwidth of the sound waves and the large delay, it is difficult to meet the requirements in short-range high-speed transmission scenarios [4]. RF communication can't be applied in the underwater working environment due to its small communication radius and low rate. Due to the existence of a blue-green permeability transmission window, underwater optical communication has become a hot spot in the research of short-distance and large-capacity underwater data transmission.

Optical MIMO systems are currently available with non-imaging receivers based on PIN, APD, and SPAD photodiodes and imaging receivers based on PD arrays or image sensors (CCD, CMOS) [5–7]. Non-imaging optical MIMO based on electro-optical signal interconversion and the use of optical energy detection to receive signals, the use of wireless communication signal processing at the electrical signal end. The technical requirements for the receiver side are becoming higher and higher to achieve high-speed omnidirectional communication, which the system need to solve the problems of energy convergence, multi-source layout synergy, and multipath effects. Therefore, such receivers are costly, complex, and less efficient systems. And with the rapid development of semiconductor technology, there is a wider choice of transmitter and receiver devices for mobile wireless optical communication systems.

The current new CCD and CMOS image sensors response speed and sensitivity are slightly lower than those of a single photodiode. Therefore, we can select a high-sensitivity and fast-response speed photodetector to form sensor arrays for imaging reception [8]. At the same time, the imaging receiver can receive the data from multiple light sources, which can obtain a high transmission rate and spectral efficiency through spatial multiplexing to compensate for the low response speed and sensitivity of a single sensor. The light-emitting arrays composed of a plurality of light-emitting elements are used as an optical transmitter, an imaging lens with a converging light effect as an optical imaging device, and each pixel of the internal image sensor at the receiving end can be regarded as a light detection element.

Imaging MIMO device is simple, based on the light intensity detection method, which determines the transmission distance. The receiving image sensor can perceive the multi-channel visible light information, so that the effective area of the received signal increases geometrically. Even if the target object moves, it is only projected in other locations of the imaging plane, resulting in good mobility. Also, detection and recognition with image processing algorithms and the non-correlated properties of imaging on different pixels provide the basis for constructing the channel matrix.

As shown in Table 1, underwater optical communication has developed rapidly and made great progress in recent years. In 2009, Marek Doniec et al. developed the AquaOptical underwater optical communication system with three optical modems, which achieved 1.2 Mbps data transmission in clear water at a communication distance of 30 m [9]. In 2010, Marek Doniec et al. developed the AquaOptical II underwater optical communication system, which achieved a data transmission rate of 2.28 Mbps using discrete pulse interval modulation (DPIM) at a communication distance of 50 m and controlled the bit error rate (BER) to 5.1 dB [10]. In 2013, a research team from Ocean University of China designed an LED-based underwater optical communication system that achieved the goal of transmitting data at a rate of 1 Mbps over a distance of 10 m [11]. In 2015, Gayathri C.B. et al. designed a transmitting system based on

ultra-bright blue LEDs and developed an enhanced photodiode-based receiving system with a data transmission rate of 1 Mbps at a communication distance of 30 m [12]. In 2016, a research team from the National Taipei University of Technology proposed a four-level pulse amplitude modulation (PAM 4) underwater wireless optical communication system based on 488 nm laser diode (LD), optical injection, and optoelectronic feedback techniques that achieve a data transmission rate of 16 Gbps at an underwater communication distance of 10 m [13]. In 2017, the Photonics Laboratory of King Abdullah University of Science and Technology used a single-mode InGaN/GaN quantum well blue light emitting LD in a TO-can package as a transmitter to achieve a laser diode visible light communication link with a data rate of 2.2 Gbps over a 12 m underwater channel [14]. In 2018, a research team from the National Taipei University of Technology proposed an underwater wireless optical communication system based on a 680 nm red VCSEL transmitter with a data rate of 25 Gbps in a 5 m high turbid harbor waterway [15]. In 2019, Prof. Nan Chi's research team at Fudan University proposed three advanced modulations based on probabilistic shaping for underwater visible light communication and employed DFT-S OFDM PS-128 QAM modulation to successfully achieve a transmission rate of 3.59 Gbps for the 1.4 m underwater VLC transmission [16]. In 2021, Professor Jing Xu's research team at Zhejiang University proposed a full-duplex (FD) underwater wireless optical communication system based on blue-green wavelength division, which can achieve a data rate of 200 Mbps at a distance of 100 m in a swimming pool [17].

Table 1. Research progress of the UWOC system

Light source/detector	Underwater distance	Data transfer rate	Modulation method	Hardware	Reference
LED-APD	30 m	1.2 Mbps	DPIM	FPGA	2009[9]
LED-APD	50 m	2.28 Mbps	DPIM	FPGA	2010[10]
LED-PMT	10 m	1 Mbps	OOK	–	2013[11]
LED-PD	30 m	1 Mbps	OOK	–	2015[12]
LD-PD	10 m	16 Gbps	PAM4	–	2017[13]
LD-APD	12 m	2.2 Gbps	NRZ-OOK	–	2017[14]
VCSEL-PD	5 m	25 Gbps	NRZ-OOK	–	2018[15]
LED-PIN	1.4 m	3.59 Gbps	DFT-S OFDM PS-128 QAM	AWG	2019[16]
LD-PMT	100 m	200 Mbps	OOK	AWG	2021[17]
LED-APD	30 m	80 Mbps	OOK	FPGA	This paper

For the performance advantages of the above photodetector devices and modulation technology, this paper considers that the transceiver must be precisely aligned when LD is used as the system light source. Based on the underwater blue and green light transmission window, the blue LED with a wavelength of 450 nm and the green LED

with a wavelength of 530 nm are used as the duplex light source at the transmitter side, and the APD arrays with high sensitivity are used as the photodetector at the receiver side. The imaging MIMO communication system is designed, and real-time signal processing is performed by an FPGA.

2 Imaging MIMO Communication System

Optical MIMO systems can be divided into imaging MIMO and non-imaging MIMO. In non-imaging MIMO, the receiver side consists of PD, APD, PIN, PMT, and other optical conversion devices, while in imaging MIMO, the receiver is not only equipped with the above devices but also with the imaging lens. Non-imaging MIMO has the advantages of a simple structure and lower cost compared to imaging MIMO, but the transmitter side of this system uses LED as the light source, which has a larger divergence angle compared to LD. If non-imaging MIMO is used in the communication system, the same LED light source is often distributed on different detectors. Non-imaging MIMO systems need to consider signal isolation and cooperative layout of multiple light sources and combine images distributed on the different detectors for subsequent data recovery to improve BER performance. This receiver is not only expensive but also complex equipment and has low system efficiency [18]. Therefore, this system chooses to use the optical imaging MIMO reception model.

The system is mainly composed of three parts: electrical signal processing, optical lens, and photoelectric conversion devices. In the imaging MIMO communication system, after the original signal is modulated, it is emitted by the LED light source arrays. The optical signal is refracted by the lens at the receiving end to form the spot, and the fiber transmits the spot coupling to the detector arrays. After the detector receives the optical signal, it performs MIMO signal detection and demodulation to obtain the original signal. The schematic diagram of the imaging MIMO system model is shown in Fig. 1.

2.1 Electrical Domain Signal Processing for Imaging MIMO Systems

At the transmitter side, the FPGA signal processing unit performs RS coding, inserts frame synchronization and bit synchronization codes, 8 B to 10 B coding, and serial/parallel conversion on the original signal to obtain the modulating signal, then it is converted to LVTTL level to drive the LED arrays, converting the electrical signal to an optical signal for transmission. At the receiving end, the FPGA performs MIMO detection on the photoelectrically converted signal to obtain each channel signal and then performs parallel/serial conversion, 8 B to 10 B decoding, the judgment of frame synchronization and bit synchronization code, and RS decoding to obtain the demodulated signal. The block diagram of the signal processing principle of the imaging MIMO system is shown in Fig. 2.

2.2 Imaging MIMO Spot Formation Principle

This system adopts the optical fiber receiving scheme of an underwater four-channel MIMO optical communication system. Four beams of distantly emitted LED light are

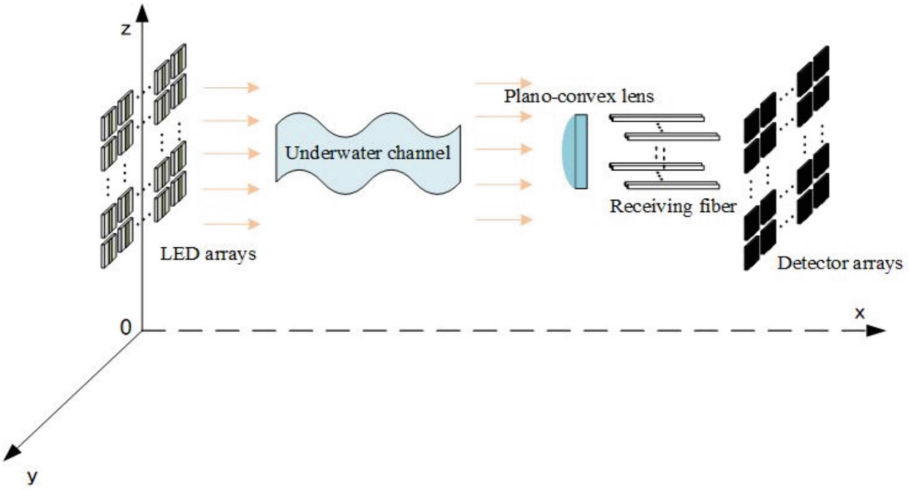

Fig. 1. Schematic diagram of the imaging MIMO system model

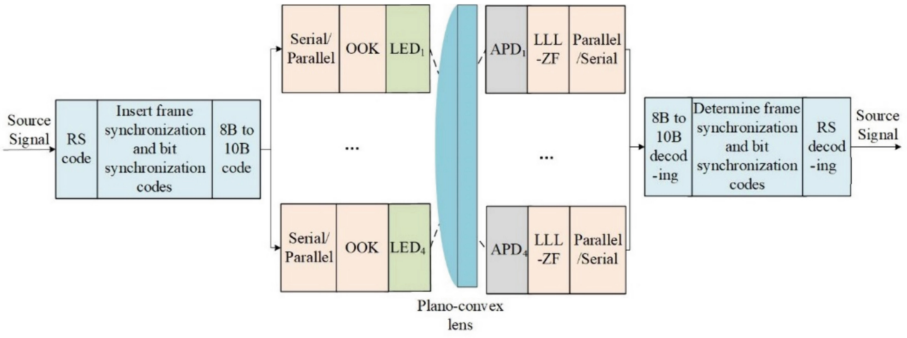

Fig. 2. Block diagram of the signal processing principle of the imaging MIMO system

directed into the receiving lens as approximately parallel light, and there will be four corresponding imaging light spots at the focal plane. The interval between the imaging light spots is very small. Therefore, four optical fibers are placed in the focal plane such that the four spots are respectively aligned to the receiving ends of the four fibers and coupled to the fiber. The other end of the receiving fiber arrays is closely aligned with four APD detectors to realize four-channel photoelectric signal conversion. The communication distance of this system is 30 m. In order to make the light source imaging in the imaging plane smaller and avoid the imaging plane light spot being larger than the receiving fiber aperture, it is necessary to ensure that four LED chips are closely arranged in each light source. This system uses the GCL-010123 plano-convex lens for receiving, which has a lens aperture of 76 mm and a focal length of 300 mm. If the interval between each light source is *d1*, the spacing between LED chips is *d2*, which, to ensure the communication performance, should make $d1/d2 > 10$. In the conditions

of an aperture of 76 mm, a focal length of 300 mm, and an object distance of 15 m, the analysis found that the four LED chip spacing should be less than 20 mm and the spacing between the four launch lights at least 160 mm, so the system design light source spacing of 200 mm. From the above parametric conditions and the geometric optical imaging equation can be expressed as:

$$1/u + 1/v = 1/f \tag{1}$$

where u, v, f are object distance, image distance, and focal length, it is known that the light source to the center of the lens angle: a = 100 mm / 15 m = 6.67 mrad, image distance v = 1/(1/0.3–1/15) m = 0.306 m, image height h = 6.67 mrad × 0.306 m = 2.04 mm. Can be used the fiber core diameter of 3 mm (including the protective layer outside diameter of 3.79 mm) for receiving fiber optics, the end of the fiber for the polished form without connectors, and the 3 mm core diameter fiber receiving field of view for 3 mm / 0.3 m = 10 mrad.

To design the four-way receiving fiber structure, we need to analyze the specific spacing of the four-way imaging light spot. When the focal length of the lens is 300 mm and the distance between fixed light sources is 200 mm, according to Eq. (1), when the object distance changes, the image distance will also change, resulting in a change in the image height. After the test, the variation curve between the spacing of the spot and the spot size at the receiving end with the transmission distance (object distance) can be obtained, as shown in Fig. 3.

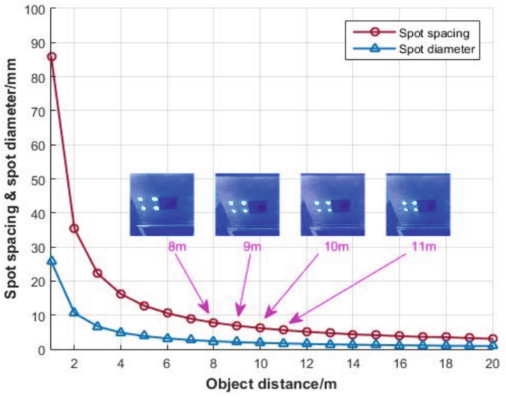

Fig. 3. The variation curve between the spacing of the spot and the spot size at the receiving end with the transmission distance (object distance)

When the object distance is fixed at 15 m and the distance between light sources is adjusted, the image height will change. The spacing of the spot at the receiving end and the variation curve of the spot size with the spacing of the light source can be obtained after the test, as shown in Fig. 4.

From the imaging spot size and spacing, the 30 m distance imaging spot center distance is 4 mm, and the spot size is about 3 mm. Using a core diameter of 3 mm

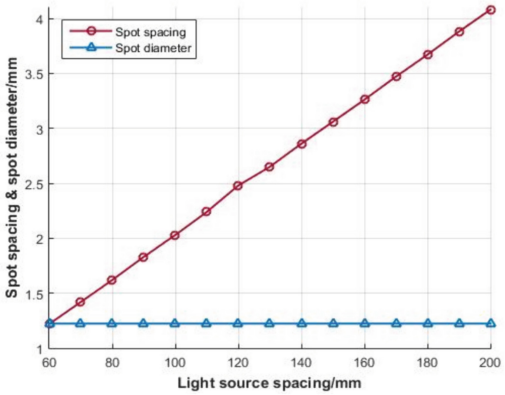

Fig. 4. The spacing of the light spot at the receiving end and the change curve of the light spot size with the spacing of the light source

for fiber reception, open a square hole with a side length of 7.6 mm, insert four fibers into the square hole, and spot glue them in place. The fiber optic fixing method uses end-polished fiber optics directly inserted into the processing hole and dispensing fixed, four fiber optics inserted into the workpiece hole to complete the fiber installation.

3 Imaging MIMO Signal Processing

The light signal emitted by the light source at the transmitter side passes through the underwater channel and then shines on the detector at the receiver side, where the APD at the receiver side converts the light signal into an electrical signal. Before the signal demodulation, in order to reduce the interference of signals from other light sources with the signal from the current light source, it is necessary to use signal detection technology on the received signal. Signal detection can be divided into two types: linear detection and non-linear detection. In the linear detection method, the flow of information from the target light source is regarded as valid information, while the rest is regarded as interference. When detecting signals from a target light source, the interference signal should be minimized or eliminated. Zero forcing (ZF) detection is among the commonly used linear detection algorithms [19]. Maximum likelihood (ML) detection belongs to the more commonly used nonlinear detection algorithms. The ML detection method calculates the Euclidean distance between the received signal vector and the product of all possible transmit signal vectors and a given channel H and finds a minimum distance. But the complexity of the ML detection algorithm increases with the modulation order and the number of antennas [20].

In this system, the light spot can be separated by imaging and the interference is relatively low, so the low-complexity linear detection algorithm is used for MIMO detection. The LLL algorithm, proposed in 1982, is an algorithm to find the approximate shortest vector of the grid in polynomial time [21]. In 2014, LLL was applied in the field of MIMO signal processing. Let $\boldsymbol{b}_1, \boldsymbol{b}_2, \ldots, \boldsymbol{b}_n \in \boldsymbol{R}^m$ be a set of bases if they satisfy the:

$$\left|\mu_{i,j}\right| \leq 1/2, 1 \leq j < i \leq n \tag{2}$$

$$\delta\left\|\mathbf{b}_{k-1}^{*}\right\|^{2} \leq \left\|\mathbf{b}_{k}^{*}\right\|^{2} + \boldsymbol{\mu}_{k,k-1}^{2}\left\|\mathbf{b}_{k-1}^{*}\right\|^{2},\ k = 2, 3, \ldots, n,\ 1/4 < \delta \leq 1 \tag{3}$$

Then this ordered set of bases ($\boldsymbol{b}_1$, $\boldsymbol{b}_2$,…, $\boldsymbol{b}_n$) is said to be the LLL statute base governed by the parameter. Where $\boldsymbol{b}_k{}^{*}$ is the corresponding Gram-Schmidt orthogonal basis, the purpose of the LLL algorithm is to transform any given basis into a set of bases with good orthogonality and as short a length as possible. The LLL-ZF detection algorithm transfers the signal to be detected from the original signal domain to the transform domain, performs ZF detection in the transform domain, and then transfers it back to the original signal domain, a process that reduces the effect of noise in the signal. The algorithm was further compared and analyzed with ZF, ML, singular value decomposition-maximum likelihood (SVD-ML), and minimum Euclidean distance-maximum likelihood (MMED-ML) detection algorithms. Among them, the SVD-ML detection algorithm performs power allocation precoding based on singular value decomposition at the transmitter side, and the MMED-ML detection algorithm performs power allocation precoding based on the minimum Euclidean distance of the received signal at the transmitter side. In this paper, we compare and analyze the BER performance of different algorithms at different signal-to-noise ratios for imaging MIMO systems with more serious speckle mixing interference, i.e., the channel condition number is 21.97, and the simulation results are shown in Fig. 5.

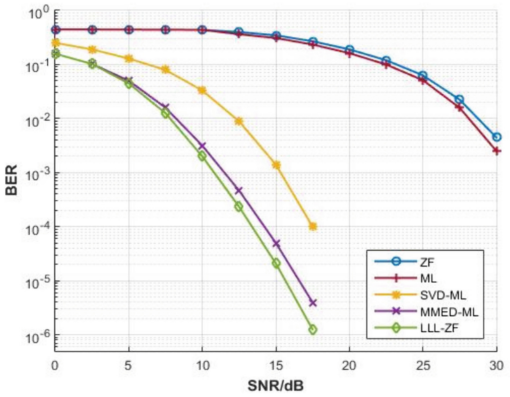

Fig. 5. BER curves of different detection algorithms under different SNR conditions

As can be seen from Fig. 5, the performances of ZF and ML are similar and worse at the channel matrix condition number 21.97. SVD-ML and MMED-ML adopt power precoding technology in the transmitter end, so their performance is better than ZF and ML. The signal-to-noise ratio (SNR) of MMSD-ML is 4 dB lower than that of SVD-ML when the BER is 10^{-3}. While the performance of the LLL-ZF and MMED-ML algorithms is similar, the LLL-ZF algorithm reduces the system complexity while improving the BER performance compared to the other detection algorithms.

4 Experiments and Analysis of Results

4.1 Experimental Setup

According to the literature [22], for light wavelengths in the 450–550 nm blue-green wavelength band, underwater propagation attenuation is minimal. Therefore, the light source at the transmitting end of the system uses blue LXR0-SR00 lamp beads and green crystal element LEDs. Blue LXR0-SR00 emits a light wavelength of 450 nm, and green crystal element LEDs emit a light wavelength of 525 nm. The imaging MIMO emitter LED arrays produce a luminous effect as shown in Fig. 6. The receiver adopts the APD model S8664-30K as the receiver detector of the system, which detects wavelengths from 320 nm to 1000 nm.

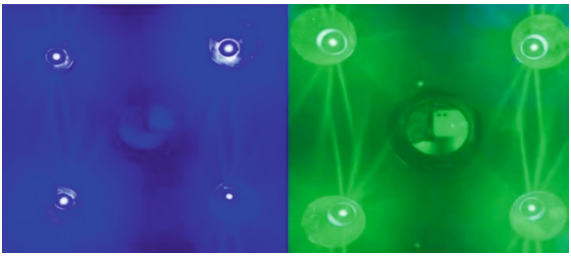

Fig. 6. Imaging MIMO transmitter LED arrays light effect

The system's real-time signal processing uses the model XC7Z020CLG400-2 FPGA as the signal processing unit, using a dual-core Corte-A9 processor with a maximum frequency of 766 MHz. Its main control chip has a working temperature of −40 °C to 100 °C, 85K logic units, 106K registers, and 220 multipliers, and its memory can reach 1GB DDR3, which can fully meet the requirements of the system for multi-channel signal processing. The imaging MIMO system structure is shown in Fig. 7.

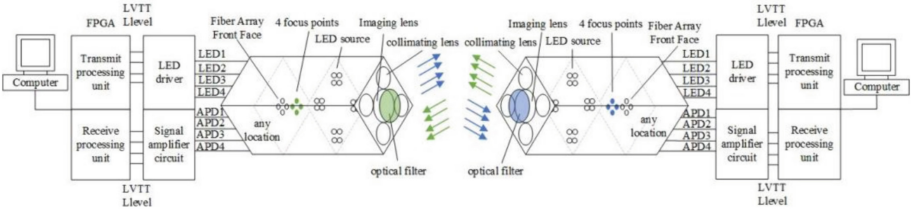

Fig. 7. Schematic diagram of the structure of the imaging MIMO system

The system structure is that the original signal input to the system, which is modulated by the transmitter using the OOK modulation technique to load the signal to be transmitted into the LED arrays at the transmitter and send it out. The optical signal is irradiated through the underwater channel to the surface of the lens at the receiving end

and passes through the lens to form a light spot, which is coupled by optical fiber and enters the detector arrays. At the receiving end, the signal undergoes LLL-ZF detection and is demodulated by the demodulator to produce the original signal.

4.2 Free Space BER Test Results at Different Distances

According to the previous analysis, as the object distance changes, the spot spacing and spot diameter at the receiving end also change. The position of the detector arrays at the receiving end is fixed, so different communication distances will form different spatial locations of the light spot, resulting in the light spot being unable to be imaged on the detector target surface, thus affecting the BER performance of the system. As shown in Fig. 8, the BER of the imaging MIMO system with different communication distances is tested, and the BER variation curve shows that the BER of the system first decreases and then increases as the communication distance increases. When the communication distance is 7–11 m, the BER of the system is about 10^{-1}, and the communication performance of the system is poor. As the communication distance continues to increase, when the communication distance is 12–24 m, the communication performance of the system is better, and at this time the system is error-free and meets the requirements of the BER for communication. However, as the communication distance continues to increase, when the communication distance reaches 25–30 m, the system BER performance will again become poor, and the BER of the system is about 10^{-2}. At this time, the system can't communicate properly. According to the experimental results and analysis, the optimal communication distance of this system is 12–24 m in free space.

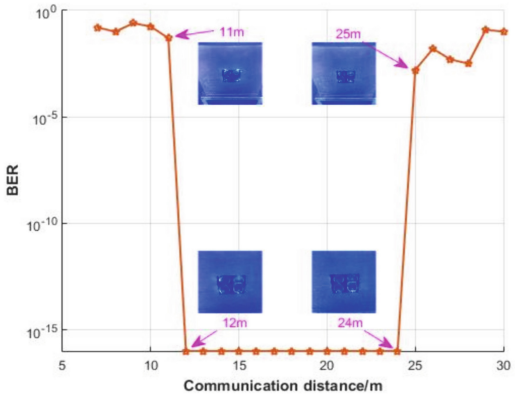

Fig. 8. Indoor BER test curve at different distances

4.3 Underwater Optical Power Test Results at Different Distances

Due to the complex environment of the underwater channel, we must consider the interference that light suffers when propagating in seawater. In the literature [23], the optical properties of seawater are divided into two types: intrinsic optical properties (IOPs) and

apparent optical properties (AOPs), where IOPs mainly include two optical parameters, the absorption coefficient and the scattering coefficient. And the influence of IOPs is mainly considered in underwater optical communication. When light propagates in the air, it will be affected by various factors in the air, such as fog or haze. The propagation of light will be hindered, and the most intuitive feeling is the darkening of the surrounding environment. Similarly, when light propagates in water, it is disturbed by various substances in the water, resulting in absorption and scattering phenomena, and in general, the attenuation coefficient can be used to describe the attenuation of light in water and expressed as [24]:

$$c(\lambda) = a(\lambda) + b(\lambda) \tag{4}$$

where $a(\lambda)$ and $b(\lambda)$ denote the absorption and scattering coefficients, respectively, and λ indicates that the attenuation coefficient is wavelength dependent. The attenuation coefficient $c(\lambda)$ varies continuously with the type and depth of the seawater. Similarly, due to the increase in communication distance, the interference in the process of light propagation will also increase, and the attenuation of optical power will also increase. Beer-Lambert Law can be used to describe the light attenuation effect in the simplest underwater environment with the expression [25]:

$$I = I_0 e^{-c(\lambda)z} \tag{5}$$

where I_0 is the power of the transmitted light, z is the distance of the transmitted light, I is the power of the received light, and $c(\lambda)$ is the attenuation coefficient.

In this paper, the power at the transmitter side is 5 w, and water quality attenuation of 0.23 dB/m tests the received optical power size at the receiver side for different communication distances, as shown in Fig. 9. As the communication distance increases, the optical power received at the receiving end tends to decrease because the attenuation of light during propagation increases with the increase in communication distance.

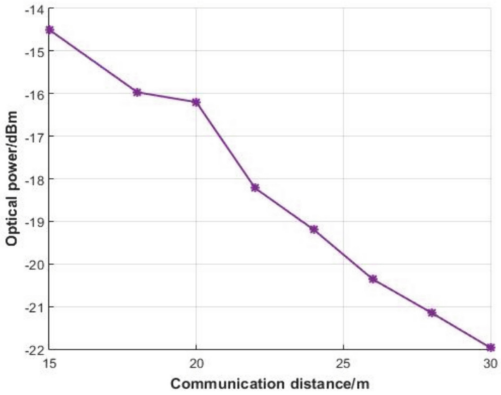

Fig. 9. Underwater optical power curve at different distances

4.4 BER Analysis Under Different Deflection Angles

Because the deflection angle is more difficult to measure, this paper uses the spot offset proportion to reverse the derivation of the deflection angle. In the experiment, when the communication distance is fixed at 13.37 m, according to Eq. (1), the angle of the light source to the center of the lens is $a = 60$ mm /13.37 m = 4.49 mrad, the image distance is $v = 1/(1/0.3–1/13.37)$ m = 0.307 m, the spot diameter is R = 4.49 mrad × 0.307 m = 1.38 mm, and the spot movement is 0.345 mm when the left deflection is 1/4. The distance between the lens and the receiving end of the light spot is 30 mm. According to the arctangent equation, the deflection angle of the light source is arctan (0.345/30) = 0.659°. When the left deflection of the light source is 8/4, the deflection angle of the light source is arctan (2.76/30) = 5.256°. Figure 10 depicts the change in deflection angle from 0.659° to 5.256° for the system BER. When the spot offset ratio is 1/2, i.e., the deflection angle is 1.318° to the left, the BER at the receiving end of the system starts to rise. When the spot offset ratio is 3/4, i.e., the deflection angle is 1.976° to the left, the BER of the system exceeds the FEC threshold. When the spot offset ratio exceeds 1, i.e., the deflection angle is more than 2.634° to the left, the BER of the system is 1.

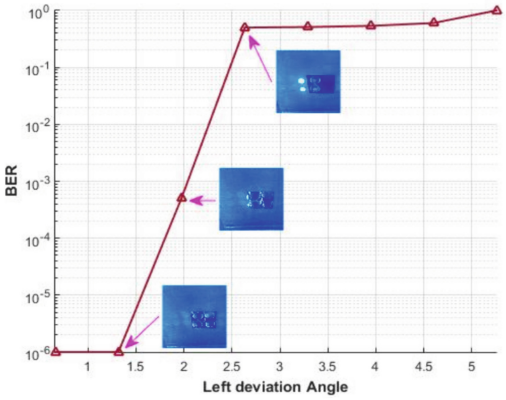

Fig. 10. BER curves at different deflection angles

5 Conclusion

For the problem of sub-channel interferences in underwater optical MIMO transmission, this paper proposes a real-time signal processing communication system based on the imaging optical MIMO reception model and proposes the LLL-ZF algorithm for MIMO detection at the receiver side. The real-time imaging optical MIMO communication system based on FPGA was developed and tested in free space and underwater, respectively. When the communication distance is 30 m, the system transmission rate can reach 80 Mbps, at the same time, the system BER is less than the FEC threshold value. The effect of different deflection angles on the BER of the system is also obtained. When the left

deflection angle is 1.318°, the BER at the receiver side of the system starts to rise, when the left deflection angle is 1.976°, the BER of the system exceeds the FEC threshold. When the left deflection angle is more than 2.634°, the BER of the system is 1. Since the position of the detector arrays at the receiving end is fixed, the next step will be to further decouple the relative position relationship between the spot and the detector arrays to extend the communication distance. The system will lay the communication foundation for underwater IoT in short-range, high-capacity transmission scenarios.

Acknowledgements. This work is supported by the National Natural Science Foundation of China under Grant (62261009), the Guangxi Natural Science Foundation (2022GXNSFDA035070), and the Innovation Project of Guangxi Graduate Education (YCBZ2022106).

References

1. Yafei, M., Zuhang, G., Shuang, J., Jinguo, Q., Yuhan, D.: Channel estimation for OFDM-based underwater wireless optical communication systems. In: Proceeding SPIE 11617, International Conference on Optoelectronic and Microelectronic Technology and Application, 116173W (2020)
2. Lanjun, L., Yonglei, Z., Pengcheng, Z., Lin, Z., Jiong, N.: Channel coding for underwater acoustic single-carrier CDMA communication system. In: Proceeding SPIE 10322, Seventh International Conference on Electronics and Information Engineering, 103222S (2017). https://doi.org/10.1117/12.2265470
3. Shijie, Z., Xinwei, C., Xiaoyan, L., Guoqi, Z., Pengfei, T.: Recent progress in and perspectives of underwater wireless optical communication. Progr. Quant. Electron. **73**, 100274 (2020). https://doi.org/10.1016/j.pquantelec.2020.100274
4. Zhou, H., Zhang, M., Wang, X., Ren, X.: Design and implementation of more than 50m real-time underwater wireless optical communication system. J. Lightwave Technol. **40**, 3654–3668 (2022)
5. Hranilovic, S., Kschischang, F.R.: A pixelated MIMO wireless optical communication system. IEEE J. Sel. Top. Quant. Electron. **12**(4), 859–874 (2006)
6. Liu, X., Doermann, D., Li, H.: A camera-based mobile data channel: capacity and analysis. In: Proceedings of the 16th ACM International Conference on Multimedia. ACM, pp: 359–368 (2008)
7. Ashok A, Gruteser M, Mandayam N, et al. Challenge: mobile optical networks through visual MIMO. In: Proceedings of the Sixteenth Annual International Conference on Mobile Computing and Networking. ACM, pp 105–112 (2010)
8. Cai, K., Jiang, M., Ma, X.: Photodetector selection aided multiuser MIMO optical OFDM imaging visible light communication system. IEEE Access **4**, 9870–9879 (2016)
9. Doniec, M., et al.: AquaOptical: a lightweight device for high-rate long-range underwater point-to-point communication. In: Proceedings IEEE OCEANS Conference, Biloxi, MS, USA, pp. 1–6 (2009). https://doi.org/10.23919/OCEANS.2009.5422200
10. Doniec, M.; Rus, D: IEEE 2010 IEEE international conference on communication systems (ICCS) - Singapore, Singapore (2010.11.17–2010.11.19)] 2010 IEEE International Conference on Communication Systems - BiDirectional optical communication with AquaOptical II. pp 390–394 (2010). https://doi.org/10.1109/iccs.2010.5686513
11. Wang, W.-P., Zheng, B.: The simulation design of LED-based close-range underwater optical communication system. In: 2013 10th International Computer Conference on Wavelet Active Media Technology and Information Processing (ICCWAMTIP), Chengdu, China, 2013, pp. 283–285, https://doi.org/10.1109/ICCWAMTIP.2013.6716649

12. Gayathri, C.B, Singh, D., Raj, N.: Design of high speed underwater optical communication using on-off keying algorithm. In: 2015 international conference on communications and signal processing (ICCSP). IEEE, pp: 1355–1360 (2015)
13. Li, C.Y., Lu, H.H., Tsai, W.S., et al.: 16 Gb/s PAM4 UWOC system based on 488-nm LD with light injection and optoelectronic feedback techniques. Opt. Express **25**(10), 11598–11605 (2017)
14. Shen, C., Guo, Y., Sun, X., et al.: Going beyond 10-meter, Gbit/s underwater optical wireless communication links based on visible lasers[C]//2017 opto-electronics and communications conference (OECC) and photonics global conference (PGC). IEEE, pp 1–3 (2017)
15. Li, C.Y., Lu, H.H., Tsai, W.S., et al.: A 5 m/25 Gbps underwater wireless optical communication system. IEEE Photon. J. **10**(3), 1–9 (2018)
16. Chi, N., Shi, M.: Enabling technologies for high-speed LED based underwater visible light communications. In: 2019 IEEE International Conference on Signal Processing, Communications and Computing (ICSPCC), Dalian, China, 2019, pp. 1–4, https://doi.org/10.1109/ICSPCC46631.2019.8960850
17. Yang, X., et al.: 100 m full-duplex underwater wireless optical communication based on blue and green lasers and high sensitivity detectors. Opt. Commun. **498**, 127261 (2021). https://doi.org/10.1016/j.optcom.2021.127261
18. Li, Y., Qiu, H., Chen, X., et al.: Spatial correlation analysis of imaging MIMO for underwater visible light communication. Opt. Commun. **443**, 221–229 (2019)
19. Wang, J, Wen, O.Y., Li, S.: Soft-output MMSE OSIC MIMO detector with reduced-complexity approximations. In: 2007 IEEE 8th Workshop on Signal Processing Advances in Wireless Communications. IEEE, 2007: 1–5
20. Zhu, X., Murch, R.D.: Performance analysis of maximum likelihood detection in a MIMO antenna system. IEEE Trans. Commun. **50**(2), 187–191 (2002)
21. Bremner M R.: Lattice basis reduction: an introduction to the LLL algorithm and its applications. CRC Press (2011)
22. Seibert, Q.: Duntley light in the Sea. J. Opt. Soc. Am. **53**, 214–233 (1963)
23. Kaushal, H., Kaddoum, G.: Underwater optical wireless communication. IEEE Access **4**, 1518–1547 (2016)
24. Xu, X., Li, Y., Huang, P., Ju, M., Tan, G.: BER performance of UWOC with APD receiver in wide range oceanic turbulence. IEEE Access **10**, 25203–25218 (2022). https://doi.org/10.1109/ACCESS.2022.3154892
25. Zhu, S., Chen, X., Liu, X., et al.: Recent progress in and perspectives of underwater wireless optical communication. Prog. Quantum Electron. **73**, 100274 (2020)